P Band UWB CSAR Vehicle Experiment and Raw Data Processing

Leping Chen, Daoxiang An, and Xiaotao Huang
College of Electronic Science and Engineering
National University of Defense Technology, Changsha, Hunan 410073, China

Abstract— In circular synthetic aperture radar (CSAR), targets are usually scanned over the complete azimuthal aperture of 360°. Thus CSAR can provide a higher image resolution, increased object information and 3-D imaging in comparison to the linear SAR system. This paper presents a low frequency ultra-wideband CSAR experiment and results. The CSAR system, operating in the P band, is based on a P band UWB SAR system integrated onboard a vehicle (IVECO). For the measurement campaign is a near field imaging, the transmitter and the receiver is bistatic, which are set on the top of the IVECO separately. A measurement campaign was conducted to investigate the performance of the low frequency UWB CSAR imaging and scattering characteristics of complex vehicle target. A CSAR imaging method, which is based on fast factorized back projection (FFBP), is proposed to focusing near field data, and the reconstructed images are cleaned out from clutter to more easily visualize the layover artifacts.

1. INTRODUCTION

Circular synthetic aperture radar (CSAR) is a SAR system whose antenna at a fixed moves along a circular trace while illuminating the interior ground region of the scanning path. By acquiring multi-angular measurements over 360°, CSAR can provide higher image resolution, increased object information and 3-D imaging in comparison to the linear SAR (LSAR) system [1, 2]. Combining with low frequency UWB signal, CSAR shows a considerable advantage to detect vehicles in the forest concealment [3]. Due to these unique properties, CSAR has been widely used in various tasks [2–4].

Attractive features of CSAR raise interest of SAR community. Several airborne Circular SAR experiments have been performed [2–4], and the potentials of CSAR have been validated.

In this article, we are primarily concerned with the empirical assessment of a vehicle target behavior under a UWB CSAR system. For this purpose, we have adopted a moving antenna, static-target scanning. A vehicle (IVECO) was exploited to acquire ground-based P-band data of various test objects. The 2D imaging results were obtained by using fast factorized back projection (FFBP). And the obtained images are cleaned out from clutter to more easily relate the physical features of the targets.

2. EXPERIMENTAL SETUP

The characteristics of near-field CSAR were experimentally investigated by utilizing the parameter values give in Table 1. The P band UWB SAR system was integrated onboard a IVECO, as shown in Fig. 1. The transmitting antenna was set on the right front of IVECO's roof, and the receiving antenna was set on the right rear of the roof. The antennas arranged in HH polarization had a height of $z_T = z_R = 4.30\,\mathrm{m}$ from the ground surface and an incident angle of $\theta_{iT} = \theta_{iR} = 12.13°$. The system was allowed up to 360° azimuthal viewing with a scanning radius of $R_g \approx 20\,\mathrm{m}$. The targets, such as a quad-trihedral (QT) and a Honda Odyssey minivan, were placed in a square of our campus, as shown in Fig. 2.

3. RAW DATA PROCESSING

In order to deal with the non-ideal circular track of the antennas and large volume data, we consider the fast factorized back projection algorithm (FFBPA), which is a direct and fast time domain algorithm. However, there is a great need for precise trace information of the antennas to apply the FFBPA.

3.1. GPS Data Processing

The trace information of our system was collected by a GPS receiver set on the center of IEVCO's roof. Before acquirement of the antennas trace, the GPS raw data need a pre-processing, such as filtering and up-sampling processing. The imaging geometry in the ground plane is shown in Fig. 3. We define Cartesian coordinates with the origin at the center of the illuminated scene. And (x, y) is denoted as the positions of GPS sensor, which is on the center of IEVCO's roof. θ_C is defined

Figure 1. The vehicle CSAR system with bistatic transmitting antenna and receiving antenna.

(a) (b)

Figure 2. Targets in the illuminated scene. (a) Quad-trihedral; (b) A Honda Odyssey minivan.

Table 1.

Parameters	Values
Center frequency	P-band
Signal bandwidth	100 MHz
Pulse repetition frequency	1000 Hz
Circle Radius	≈ 20 m
Height	4.30 m
Width of pulse	200 ns

as the azimuth angle of the GPS sensor. l and d are the distances between the antenna and GPS sensor in tangential and radial directions. Thus we could get the transmitter and receiver positions, which can be expressed as

$$\begin{bmatrix} x_T \\ y_T \end{bmatrix} = \begin{bmatrix} x \\ y \end{bmatrix} + \begin{bmatrix} \cos(\theta_C) & \sin(\theta_C) \\ \sin(\theta_C) & \cos(\theta_C) \end{bmatrix} \begin{bmatrix} l \\ -d \end{bmatrix} \tag{1}$$

And

$$\begin{bmatrix} x_R \\ y_R \end{bmatrix} = \begin{bmatrix} x \\ y \end{bmatrix} + \begin{bmatrix} \cos(\theta_C) & \sin(\theta_C) \\ \sin(\theta_C) & \cos(\theta_C) \end{bmatrix} \begin{bmatrix} -l \\ -d \end{bmatrix} \tag{2}$$

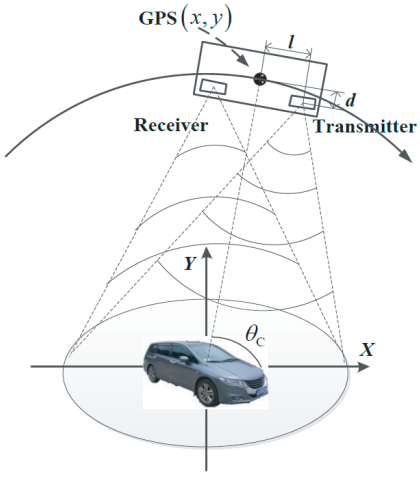

Figure 3. Subaperture imaging geometry.

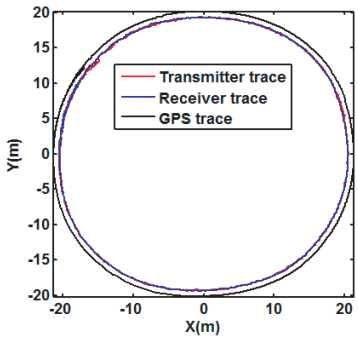

Figure 4. The traces of CSAR system.

3.2. Implementation

Based on the FFBPA for the linear SAR [5], the implementation of the FFBPA for the CSAR can be divided into three steps, as Fig. 4 shown. The processing is to first segment the entire aperture into several subapertures, then individually process each subaperture by the FFBPA, thus forming subimages, and finally combine all the raw images by polar-to-Cartesian interpolation. One thing to note is that the subapertures can be overlapped to obtain more subapertures in different azimuth direction for motion compensation and CFAR detection. And the other thing to note is that there are two strategies for combining of subimages. One is to add them together coherently to retain the information of phase. The other one is noncoherent accumulation, which can achieve the better final image than coherently processing the entire aperture [6]. In Section 4, we will present the imaging results by these two strategies.

4. EXPERIMENTAL RESULTS

4.1. Imaging of a Quad-trihedral

In the first experiment, a QT with side lengths of 75 cm was selected as targets, as shown in Fig. 2(a). With such geometry, a QT is able to exhibit strong returns from any azimuth. Fig. 6 shows the ground plane images by coherent processing and noncoherent processing, respectively. As expected, the QT represents quite high reflections due to its corner structure. And the coherent result has a better spatial resolution, while the noncoherent result achieves a better final image.

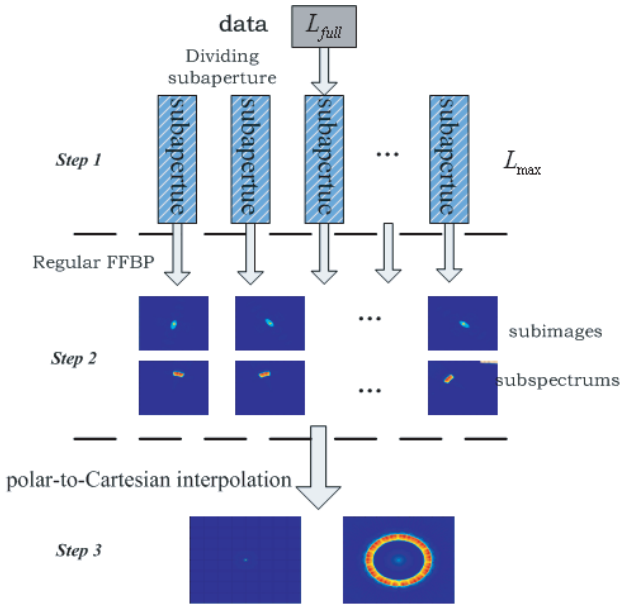

Figure 5. The implementation of the FFBPA for CSAR.

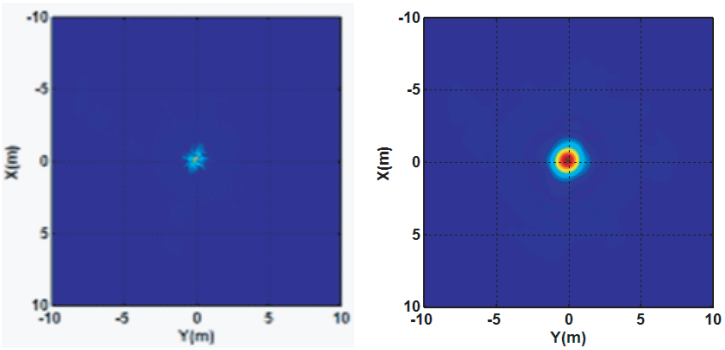

(a) (b)

Figure 6. Results for the first experiment. (a) Imaging by coherent processing; (b) Imaging by noncoherent processing.

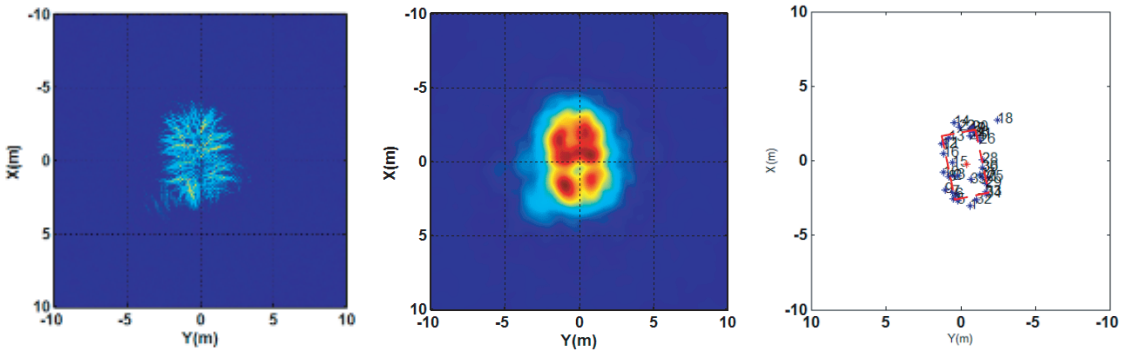

(a) (b) (c)

Figure 7. Results for the first experiment. (a) Imaging by coherent processing; (b) Imaging by noncoherent processing; (c) Extracting information for attributed scattering centers.

4.2. Imaging of a Honda Odyssey Minivan

In the second experiment, a Honda Odyssey minivan was scanned as shown in Fig. 2(b). The car has dimensions of ($4810L \times 1802W \times 1570H$ mm) causing a near-field illumination under a LOS distance of 20.5 m. The coherent imaging result is shown in Fig. 7(a) and the noncoherent one is shown in Fig. 7(b). The strong reflections are to be concentrated on the sides of the car for the multipath bounce between the lateral side and the ground place. As shown in Fig. 7(c), it's seen that the minivan's shape is almost outlined together with nearly accurate shape (red dash box).

5. CONCLUSION

A low frequency CSAR experiment has been performed using a P band radar system which was carried on an IVECO. The results obtained show that the CSAR system works well. And the imaging performance of P band CSAR is investigated by illuminating man-made targets. An airborne experiment based on this system will take place in the future. We will focus on researches of wide field imaging and target recognition.

ACKNOWLEDGMENT

This work was supported by the National Natural Science Foundation of China (NSFC) under Grants 61571447 and 61372161.

REFERENCES

1. Knaell, K. K. and G. P. Cardillo, "Radar tomography for the generation of three-dimensional images," *IEE Proceedings — Radar, Sonar and Navigation*, Vol. 142, No. 2, 54–60, 1995.
2. Ponce, O., P. Prats, M. Rodriguez-Cassola, R. Scheiber, and A. Reigber, "Fully polarimetric high-resoution 3-D imaging with cirular SAR at L-band," *IEEE Transactions on Geoscience and Remote Sensing*, Vol. 52, No. 6, 3074–3090, 2014.
3. Frölind, P., A. Gustavsson, M. Lundberg, et al., "Circular-aperture VHF-band synthetic aperture radar for detection of vehicles in forest concealment," *IEEE Transactions on Geoscience and Remote Sensing*, Vol. 50, No. 4, 1329–1339, 2012.
4. Soumekh, M., "Reconnaissance with slant plane circular SAR Imaging," *IEEE Transactions on Image Processing*, Vol. 5, No. 8, 1252–1265, 1996.
5. Ulander, L. M. H., et al., "Synthetic-aperture radar processing using fast factorized back-projection," *IEEE Transactions on Aerospace and Electronic Systems*, Vol. 39, No. 3, 760–776, March 2003.
6. Dungan, K. E. and J. W. Nehrbass, "Wide-area wide-angle SAR focusing," *IEEE A&E Systems Magazine*, Vol. 29, No. 1, 21–28, 2014.